Machine learning quantum-chemical bond scission in thermosets under extreme deformation

Zheng Yu[1] and Nicholas E. Jackson[1, a)]

Department of Chemistry, University of Illinois at Urbana-Champaign, Urbana, Illinois, 61801, USA

Despite growing interest in polymers under extreme conditions, most atomistic molecular dynamics simulations cannot describe the bond scission events underlying failure modes in polymer networks undergoing large strains. In this work, we propose a physics-based machine learning approach that can detect and perform bond breaking with near quantum-chemical accuracy on-the-fly in atomistic simulations. Particularly, we demonstrate that by coarse-graining highly correlated neighboring bonds, the prediction accuracy can be dramatically improved. Compared to existing quantum mechanics/molecular mechanics methods, our approach is approximately two orders of magnitude more efficient and exhibits improved sensitivity towards rare bond breaking events at low strain. The proposed bond breaking molecular dynamics scheme enables fast and accurate modeling of strain hardening and material failure in polymer networks, and can accelerate the design of polymeric materials under extreme conditions.

a)Email:jacksonn@illinois.edu

Thermoset polymers crosslinked by covalent bonds using curing agents form stable three-dimensional network structures with almost infinite molecular weight. Depending on the crosslinking density, the mechanical strength and toughness of thermosets can be improved remarkably and even maintained at high temperatures, making them high potential matrix materials for fiber-reinforced composites appearing in the automotive, aerospace, aviation, textile, construction, marine and sports industries.[1] Although the thermal and mechanical behaviors of polymer networks have been well studied by molecular dynamics (MD) simulations, these studies have been primarily limited to the elastic and strain softening regimes.[2–11] Further modeling of hardening and failure, which are critical for degradation, recycling, and extreme applications,[12–17] require the ability to include bond scission in classical MD. While approaches such as reactive empirical bond order, breakable bond potential, and ReaxFF allow bond breaking, they typically require extensive *ad hoc* calibration and can exhibit poor performance for materials outside of their training sets.[18–21]

The most accurate representation of bond breaking relies on quantum mechanical (QM) calculations that are rigorous solutions to the Schrödinger equation. Due to the computational cost of QM, combined quantum mechanics/molecular mechanics (QM/MM) have been developed, in which QM is performed only on a small subsystem of the most interest while the remaining majority is treated with MM.[22–24] For constantly detecting bond breaking during materials deformation, Barr, Kedziora, Ecker, et al. developed an alternating MD and QM simulation scheme.[25] Specifically, MD simulations performed on the entire system are repeatedly stopped to check whether a bond breaking event is likely to occur. If a bond length surpasses a certain threshold, a local structure surrounding the bond (QM cluster) is extracted for QM geometry optimization. Whether a bond breaks or not can be identified based on the final distance between the two atoms involved in the bond after optimization. For example, as employed in the reference,[25] a bond is empirically identified as broken if the distance is 1.5 times larger than its equilibrium bond length. For the record, this method developed by Barr, Kedziora, Ecker, et al. is not the traditional QM/MM, which we will refer to as Barr's method hereinafter.

However, for bond breaking detection under extreme deformation, a large QM cluster size is required to minimize finite size effects in amorphous systems.[25,26] This QM cluster size is associated with the lengthscale of the dynamical and mechanical heterogeneities which will increase with the enhanced thermodynamic stability of glassy polymers.[27–29] In addition, the bond length threshold for triggering QM calculations needs to be small enough to include all potential broken

bonds. These two requirements dramatically increase the QM computational cost and therefore limit the timescales that atomistic simulations can explore. Recently, machine learning (ML) has demonstrated the ability to reproduce the results of QM calculations with substantially reduced computational cost.[30–37] In this work, we propose a hybrid ML-molecular modeling approach that can modify bonding topology on-the-fly in atomistic simulations with near quantum-chemical accuracy. Our approach maintains the efficiency of classical MD and can extend the accessible strain rates in simulations of thermosets by at least two orders of magnitude compared to Barr's method.

We begin by considering the bond breaking of an archetypal epoxy polymer network, diglycidyl ether of bisphenol A (DGEBA) cured by methylene dianiline (MDA). A cubic simulation box containing 432 DGEBA and 216 MDA molecules, i.e., 27,432 atoms in total, is created with periodic boundary conditions in all three dimensions. To collect data for training the ML model, we utilize MD simulations (OPLS-AA)[38] to generate a variety of polymer configurations with different crosslinking densities and thermal and deformation histories, as summarized in Table 1 of the Supplementary Material (SM).[39–45] Based on bond length or energy, local structures that are suspected to contain broken bonds are then selected from the MD configurations for further QM optimization, similarly as in Barr's method. In the QM calculation, a constraint is applied in the outer shell of the cluster to maintain the local stress from the large MD structure, i.e., atoms in the constrained region are kept frozen and atoms in the inner region are fully optimized based on quantum-chemical forces, as illustrated in Fig. 1A. We compare the density functional theory (DFT) method PBEh-3c and the semi-empirical tight-binding method GFN2-xTB in our testing, observing similar results,[46,47] leading us to apply the more efficient xTB for generating ML training data in this work. Any further improvement in the quantum chemistry methods for the QM calculation can be readily included in our workflow. More details of the methodology can be found in the SM. In total, $\sim$112k data points with QM-based bond breaking detection are generated.

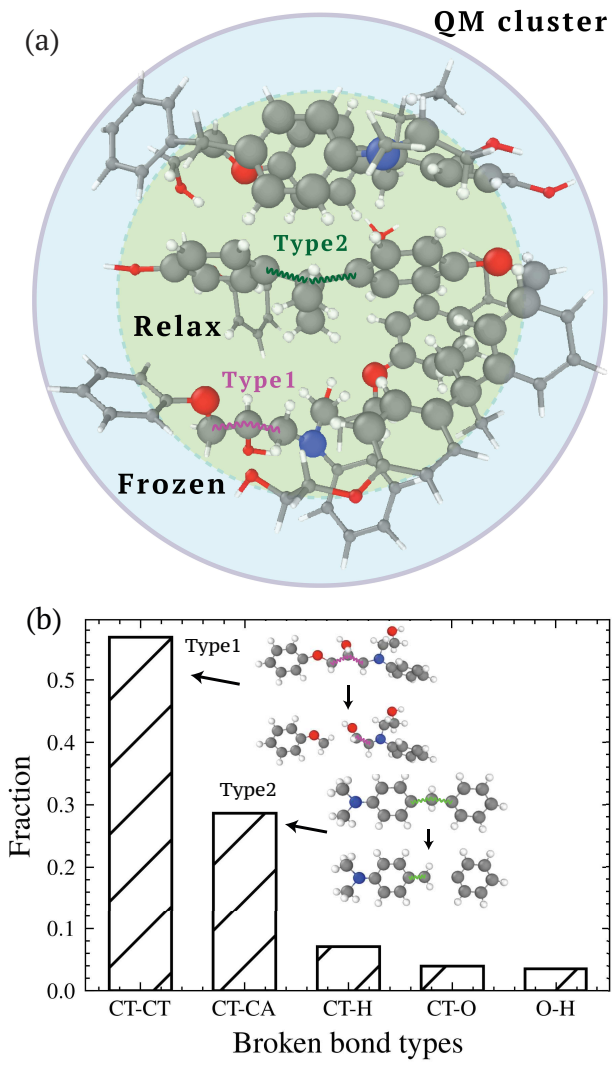

FIG. 1. (a) A representative local structure extracted from MD configurations of highly crosslinked DGEBA cured by MDA (DGEBA+MDA) for QM geometry optimization. To constrain the local stress, atoms located in the outer shell (represented by the tiny beads connected by sticks) are kept frozen during the optimization, while the atoms in the inner region (represented by the big beads) are free to relax. For clarity of visualization, smaller cluster cutoffs are used to generate the image, resulting in fewer included atoms than in actual QM calculations. (b) Fractions of bonds types that are broken during the QM (xTB) geometry optimization. Bond breaking occurs predominantly at the 'CT-CT' (Type 1) and 'CT-CA' (Type 2) motifs. The bond types involving H are associated with the dominant bond breaking as neighbor exchanges.

After QM optimization on the large library of local structures, we study the statistics of bond breaking events in DGEBA-MDA. First, we observe that bond breaking in the thermoset is dominated by only two bond types. As shown in Fig. 1B, around 60% of bond breaking occurs in

type 'CT-CT', which is the carbon (sp3)-carbon (sp3) bond along the backbone of cured DGEBA, and 30% (40% in PBEh-3c) is of type 'CT-CA' denoting the carbon (sp3)-carbon (aromatic) bond connecting the benzene rings in DGEBA and MDA. The chemical environments of the two bond types are shown in Fig. 1. The remaining bond breaking events are neighbor exchanges involving H atoms or unstable 'CT-O' bonds (observed in xTB but not in PBEh-3c) associated with the major bond breaking types. As these minor events minimally affect strain response, we only need to address the dominant two bond types, denoted as Type 1 and 2. Note that other bond types can be stretched more strongly than Type 1 in MD deformation simulations (in Fig. S1 of SM) but remain intact during QM optimization, reaffirming that classical potentials are unreliable for describing chemical bonding under large local distortion.

Bond length and stretching energy are natural descriptors to quantify bond distortion. After identifying the dominant bond types in the rupture of DGEBA-MDA, it is worth investigating how well the two features can predict QM bond breaking under deformation. Figure 2A shows the probability distributions of normalized bond lengths for broken and unbroken bonds of Type 1 and Type 2. The normalized bond length is defined as $(l - l_o)/l_o$, where l_o is the equilibrium bond length and l the instantaneous length. In general, the unbroken bond distribution mainly occupies the small bond lengths, whereas the broken bond distribution occupies the large bond lengths ($\Delta l/l_o$>0.1). Notably, we observe a large overlap region where bond scission can and cannot occur. For instance, at $\Delta l/l_o \sim 0.22$, the probability of bond breaking is around one half for both Type 1 and Type 2. The average bond breaking probability remains zero until $\Delta l/l_o \sim$0.1 and increases almost linearly with further extension, as shown in the Fig. S2 of the SM. Based on these types of distributions, previous studies using a length threshold of $\Delta l/l_o = 0.16$ in the same system would miss $\sim$1/4 of broken bonds at smaller bond lengths.[25] Note that using a smaller value of the bond length threshold avoids this problem, but significantly increases the number of triggered QM calculations, further slowing down the MD simulation.

Interestingly, we find that bond breaking does not necessarily occur at the triggering bond that possesses the largest bond length or stretching energy in the static local structure. Figure 3 shows the distance distributions from the actual broken bonds to the triggering bond (at the center of the cluster) in three different cases. For the case with cutoff=8 Å and inner cutoff=6.5 Å, we notice a main peak around zero, representing the breaking of the triggering bond. We also observe a secondary peak around 2 Å. By examining configurational snapshots, we find that this secondary peak represents the breaking of the nearest neighbor bond to the triggering bond. The chemical

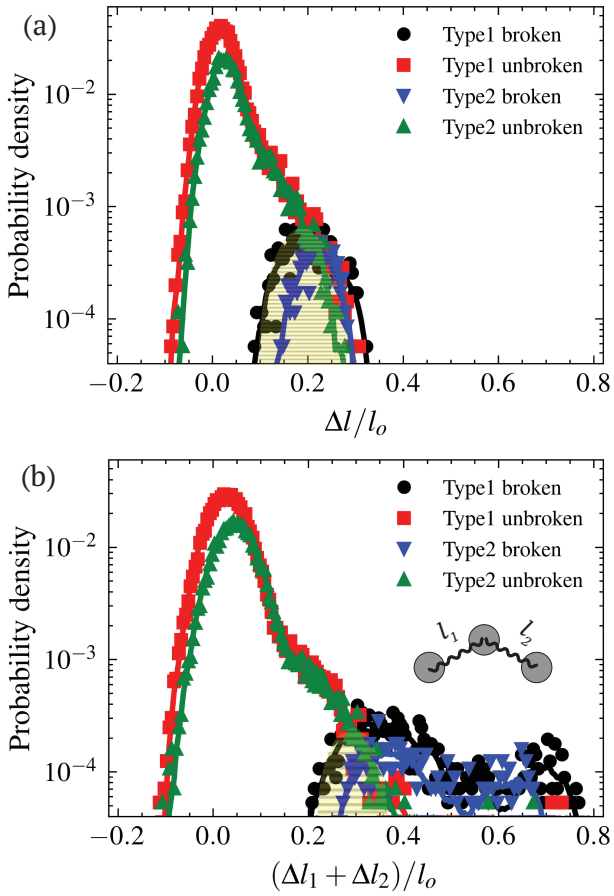

FIG. 2. (a) Distributions of normalized bond lengths for broken and unbroken bonds. The shadow represents an overlap region of bond lengths where broken and unbroken bonds co-exist. (b) Same plot as (a) but based on coarse-graining (CG) neighboring bonds, i.e., the CG bond breaks if either bond breaks. The overlap region is reduced significantly.

environment in Fig. 1 shows that each bond of the two types only has one unique neighboring bond in this system. In addition, there are a smaller fraction of broken bonds at the medium range from 3 to 6.5 Å, and some even at the constrained interface. To study whether the results are caused by the finite size of the QM regions, we extend the MM cutoff to 10 Å and the QM cutoff to 8.5 Å on the same MD configurations. As shown in the middle panel of Fig. 3A, the results of the larger cluster are nearly identical to the smaller cluster, except they exhibit more bond breaking within 8-10 Å due to the larger cutoffs.

To further validate the bond breaking events away from the trigger bond, we deliberately extract the local structures associated with the “unintentionally" broken bonds at the center of the QM re-

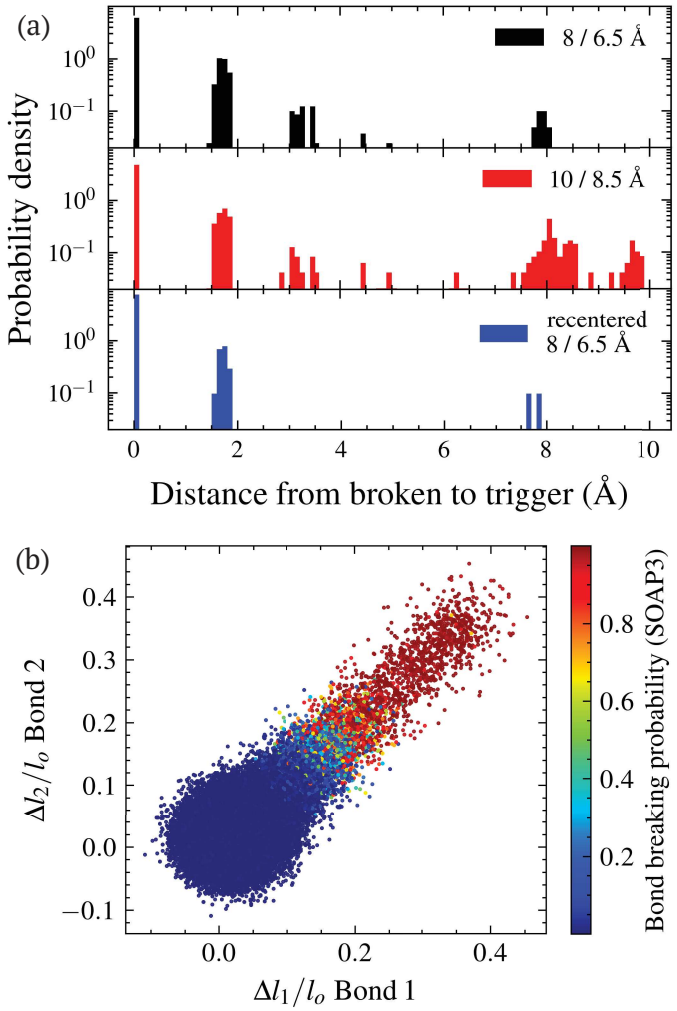

FIG. 3. (a) Distributions of distances from the actual broken bonds in QM optimization to the triggering bonds (the most stretched) in the local structures. The top two panels show results using different cutoff distances in the QM cluster. The bottom panel shows results of QM optimizations with those non-trigger broken bonds recentered in the cluster. The persistence of the peak around 2 Å indicates that neighboring bonds compete with each other in releasing the local stress, causing intrinsic noise in bond breaking predictions. (b) Strong correlation of bond lengths between neighboring bonds. The color represents the bond breaking probability predicted by the SOAP3 model.

gion, and rerun the shell-constrained QM optimization. As shown in Fig. 3A, the bond breaking occurring in the 3 to 6.5 Å range disappears with recentering. Moreover, the bond breaking occurring near the constrained interface still exists with almost the same magnitude, suggesting that they are probably caused by spurious stresses induced by the fixed boundary and should not be counted. Most importantly, the recentering results in similar main and secondary peaks, suggest-

ing that there is an intrinsic uncertainty of bond breaking between the neighboring bonds in QM calculations. After further analysis, we find that the bond lengths of the neighboring bonds are highly correlated due to sharing very similar local environments, as shown in Fig. 3B, and this local stress correlation is dominant compared to longer range correlations at large strain (in Fig. S8 of SM). This strong correlation between two neighboring bonds suggests that we could treat them together as a coarse-grained (CG) bond. As shown in Fig. 2B, the overlap regime of broken and unbroken bonds can be largely reduced based on redefinition of a CG bond capturing both neighboring bonds as the average of the two bond distortions.

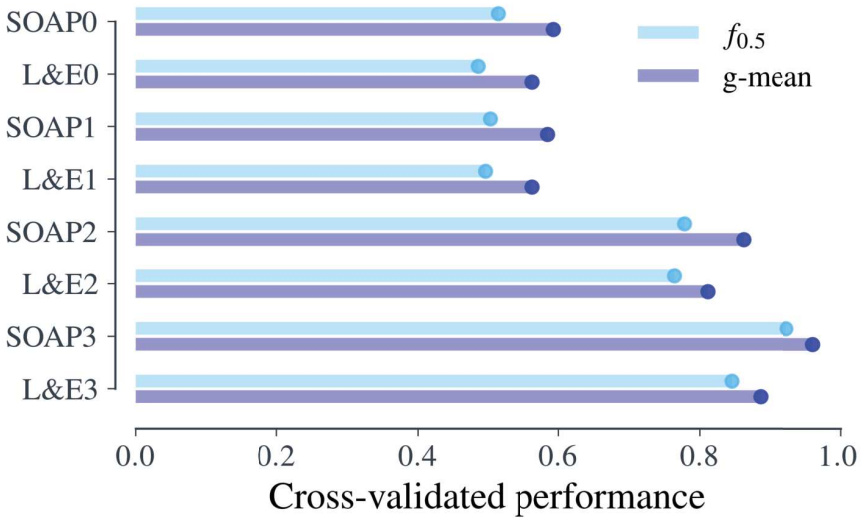

FIG. 4. ML model comparison based on cross validated $f_{0.5}$ and g-mean. 'SOAP' represents models trained based on SOAP descriptors and 'L&E' represents models trained based on only bond length and energy. The number '0' means models trained by raw data from QM optimization, '1' means models trained by data removing those with bond breaking occurring near the constrained interface, '2' means models trained by data with relabeling the output of neighboring bonds, '3' means models trained by data with CG neighboring bonds.

Based on these insights, we develop ML models for detecting bond breaking in DGEBA-MDA. Besides bond length and stretching energy, we also employ the Smooth Overlap of Atomic Positions (SOAP) descriptor,[48,49] which represents a Gaussian smeared local atomic density based on spherical harmonics and radial basis functions, with hyperparameters optimized by Bayesian optimization.[50] The models based on SOAP are trained with the support vector machine (SVM) with the radial basis function kernel.[51] The models based solely on bond length and energy ('L&E') are trained with the logistic regression with l_2 regularization.[52] Because of the bond

breaking complexity in QM optimization of finite size clusters, we design four ML models trained by different preprocessed datasets. 'Model 0' (including 'SOAP0' and 'L&E0') denotes the model trained by the raw data collected from the QM calculations. 'Model 1' denotes the model trained by removing data with bond breaking occurring near the constrained interface. 'Model 2' denotes the model trained by data with relabeling the output of neighboring bonds, i.e., once a bond breaks, its neighboring bond is labeled as broken too. 'Model 3' denotes the model trained by coarse-graining the two neighboring bonds into one, i.e., the CG bond breaks if either of the two neighboring bonds breaks while the inputs are averaged. To precisely characterize the performance of different models for this highly imbalanced classification ($\sim$1% of bonds break in the dataset), we apply the F-score $f_\beta = (1+\beta^2)\text{precision}\cdot\text{recall}/(\beta^2\text{precision}+\text{recall})$ with $\beta = 0.5$ to reduce false bond breaking and g-mean (geometry mean of class wise sensitivity) for hyperparameter optimization and model evaluation.[53] $f_{0.5}$ and g-mean both range from 0 for wrong classification (e.g., assigning all to be unbroken) to 1 for perfect classification. Note that traditional resampling techniques for imbalanced classification should not be applied, because they would increase false bond breaking and artificially make materials more fragile. Further description of the ML methods is included in SM.

Figure 4 summarizes the cross-validated performances of different ML models in predicting bond breaking. In general, the models trained with bond length and energy only have slightly lower $f_{0.5}$ and g-mean than those trained with SOAP based on the same prepossessing treatment. However, as shown in Fig. S11 of SM, bond length and energy fail to predict the bond breaking probability correctly under large strain > 0.85, likely due to the increased length scales of stress correlations. These results suggest that bond length and energy are relevant structural features for bond breaking detection, but lack the information of local environments required for highly strained conditions. Model 1 (including SOAP1 and L&E1) have similar scoring as Model 0 based on raw data. Thus, removing data with bond breaking near the constrained interface does not improve the prediction, possibly because the number of removed data is too small. Model 2 and Model 3, by addressing the intrinsic uncertainty in bond breaking between a pair of neighboring bonds, improve the model performance by more than 50% compare to Model 0. Particularly, the SOAP3 model has the highest prediction scoring with $f_{0.5}$=0.923 (std=0.02) and g-mean=0.960 (std=0.01), showing that this physics-informed machine learning model nearly reproduces the quantum-chemical accuracy.

Next, we design a Machine Learning based Adaptable Bond Topology (MLABT) simulation

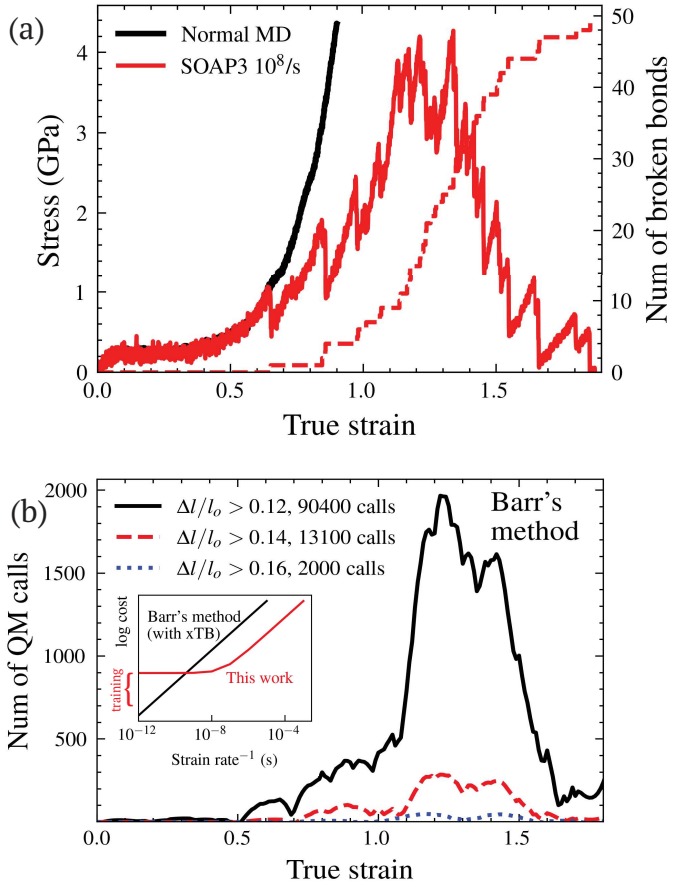

FIG. 5. (a) Stress strain curve of highly crosslinked DGEBA+MDA simulated by normal MD and MLABT at a strain rate 10^8/s. The dashed line shows the corresponding number of broken bonds in MLABT. (b) Estimated number of QM calls required for simulating the polymer deformation with Barr's method as a function of strain for three different triggering thresholds. The estimates are made based on the MLABT with SOAP3 and the total numbers of calls are given in the legend. Note that increasing the checking frequency or decreasing the strain rate will proportionally increase the number of QM calls. The inset shows the estimated computational cost between our method and the Barr's method with xTB, additional details of which are provided in the SM.

scheme implemented with MD. MLABT frequently scans all the bonds (two types herein) in an MD simulation and modifies the bonding topology on-the-fly if there are bonds predicted broken by the ML model. Note that in the CG bond definition of Model 3, only the real bond with a longer length is cut in the atomistic MD simulation. Figure 5 shows the stress strain curves simulated by MLABT and the corresponding number of broken bonds during deformation with a strain rate of 10^8/s and a check frequency of every 1 ps. It can be seen that the stress response

in our method remains the same as in normal MD until the first bond breaks around strain$\sim$0.65 during strain hardening, and after this, stress increase slows down deviating from the normal MD curve along with more bonds broken. The stress reaches a fluctuating maximum resulting from a rapid increase of broken bonds around a strain of 1.1-1.4, and eventually the material fails around strain$\sim$1.8. Snapshots showing the atomic details from the trajectory can be found in Fig. S9 of the SM. Note that strain$\sim$0.65 showing the first bond breaking is very close to the lowest strain=0.70 we observe in QM optimization that has bond breaking, suggesting satisfactory extrapolation ability of the model to unseen configurational space. The previous study (Barr, Kedziora, Ecker, et al.) reported a higher value ($\sim$0.9) of such strain,[25] suggesting that Barr's method using a relatively high threshold of bond length (for efficiency) misses the bond breaking at early stages (as shown in Fig. 2A) compared to complete scanning in MLABT. Direct comparison of our simulation results to experiments is difficult due to the large difference in time and length scales. Compared to previous simulation works, although the simulated elastic modulus and yield stress are in general agreement,[9,54] the plastic behavior involving bond breaking might differ reasonably due to differences in chemical environments and simulation methods.[55] More discussions are included in Sec. S5 of the SM.

Furthermore, we compare the efficiency of our approach and Barr's method for simulating thermoset deformation. Based on the deformed structures from the MLABT simulations, we estimate the number of QM calls required in Barr's method for simulating complete thermoset deformation. As shown in Fig. 5B, the number of QM calls increases with applied strain showing a similar trend as stress response. In addition, the number of QM calls increases exponentially when lowering the triggering threshold for thorough bond breaking detection. The inset of Fig. 5B compares estimated cost scaling with strain rate between the two methods. Although MLABT requires some QM calls ($\sim$4000) for training the ML model, its cost scales as classical MD because no QM calculations are needed after training, whereas the cost of Barr's method scales faster due to the expensive QM calculation. Using the same computational cost for simulating a strain rate of 10^9/s by Barr's method, our approach can roughly simulate a strain rate of 10^7/s. Note that the difference will be larger if using DFT for QM calculations or a larger QM cluster. A description of the cost estimate is included in Sec. S5 of SM. The MLABT model, once trained, can also be applied repeatedly without additional QM calculation cost, which is an important benefit of ML models.

In summary, we develop a physics-informed ML method that can detect and implement bond breaking with QM accuracy in atomistic MD simulations of polymer networks under large defor-

mation. We discover that by coarse-graining highly correlated neighboring bonds, the intrinsic uncertainty in bond breaking can be avoided and the prediction accuracy is improved significantly. This implies that our approach without modification can be applied in fully CG simulations. We also find that although bond length and energy alone can predict bond breaking accurately at low strains, the model including SOAP descriptors is more reliable at extreme strains.

Compared to the previous Barr's method, our ML-based approach exhibits two evident advantages: efficiency and completeness. MLABT is almost as efficient as classical MD once the model is trained, and the number of QM calculations needed for training is also much smaller than that for Barr's method. Unlike Barr's method selecting bonds above a threshold, MLABT scans all the bonds in the system and therefore it is able to detect rare bond breaking even under smaller deformation. However, our method still suffers from the discrete nature of bond breaking and associated energy description, resulting in discontinuity in the stress response, i.e., sudden drops immediately after bonds break, as shown in Fig. 5A. Future work will focus on including more complete chemical space and mechanical space (shear) to MLABT for applications in different materials and diverse situations. We believe that MLABT provides an improved solution for accurate modeling of polymer deformation and accelerates the design of polymeric materials under extreme conditions.

SUPPLEMENTARY MATERIAL

See the supplementary material for more details of the computational methods and the results of the deformation simulations by MLABT.

ACKNOWLEDGMENTS

This work was supported by the National Science Foundation Chemical Theory, Models, and Computation division under Award No. CHE-2154916.

REFERENCES

[1]J. S. Jayan, S. Appukuttan, R. Wilson, K. Joseph, G. George, and K. Oksman, in *Fiber Reinforced Composites*, Woodhead Publishing Series in Composites Science and Engineering, edited

by K. Joseph, K. Oksman, G. George, R. Wilson, and S. Appukuttan (Woodhead Publishing, 2021) pp. 1–24.

[2]C. Wu and W. Xu, Polymer **47**, 6004 (2006).

[3]C. Li and A. Strachan, Polymer **52**, 2920 (2011).

[4]A. Shokuhfar and B. Arab, J Mol Model **19**, 3719 (2013).

[5]J.-L. Barrat, J. Baschnagel, and A. Lyulin, Soft Matter **6**, 3430 (2010).

[6]A. Aramoon, T. D. Breitzman, C. Woodward, and J. A. El-Awady, J. Phys. Chem. B **120**, 9495 (2016).

[7]X. Wu, A. Aramoon, and J. A. El-Awady, J. Phys. Chem. B **124**, 11928 (2020).

[8]C. Li and A. Strachan, Journal of Polymer Science Part B: Polymer Physics **53**, 103 (2015).

[9]A. Vashisth, C. Ashraf, C. E. Bakis, and A. C. T. van Duin, Polymer **158**, 354 (2018).

[10]R. A. Riggleman, H.-N. Lee, M. D. Ediger, and J. J. de Pablo, Soft Matter **6**, 287 (2010).

[11]J. Fan, A. Anastassiou, C. W. Macosko, and E. B. Tadmor, Polymer **196**, 122477 (2020).

[12]M. J. Mullins, D. Liu, and H. J. Sue, in *Thermosets (Second Edition)*, edited by Q. Guo (Elsevier, 2018) pp. 35–68.

[13]W. Post, A. Susa, R. Blaauw, K. Molenveld, and R. J. I. Knoop, Polymer Reviews **60**, 359 (2020).

[14]N. Xu, B. Wang, Z. An, Y. Liu, L. Liu, Z. Hu, and Y. Huang, Chem. Mater. **34**, 4732 (2022).

[15]C. P. Buckley, J. Harding, J. P. Hou, C. Ruiz, and A. Trojanowski, Journal of the Mechanics and Physics of Solids **49**, 1517 (2001).

[16]C. W. Barney, Z. Ye, I. Sacligil, K. R. McLeod, H. Zhang, G. N. Tew, R. A. Riggleman, and A. J. Crosby, Proceedings of the National Academy of Sciences **119**, e2112389119 (2022).

[17]R. K. Bay, T. Zhang, S. Shimomura, M. Ilton, K. Tanaka, R. A. Riggleman, and A. J. Crosby, Macromolecules **55**, 8505 (2022).

[18]J. Tersoff, Phys. Rev. B **37**, 6991 (1988).

[19]M. Tsige and M. J. Stevens, Macromolecules **37**, 630 (2004).

[20]A. C. T. van Duin, S. Dasgupta, F. Lorant, and W. A. Goddard, J. Phys. Chem. A **105**, 9396 (2001).

[21]M. J. Stevens, Macromolecules **34**, 2710 (2001).

[22]A. Warshel and M. Levitt, Journal of Molecular Biology **103**, 227 (1976).

[23]U. C. Singh and P. A. Kollman, Journal of Computational Chemistry **7**, 718 (1986).

[24]M. J. Field, P. A. Bash, and M. Karplus, Journal of Computational Chemistry **11**, 700 (1990).

[25]S. A. Barr, G. S. Kedziora, A. M. Ecker, J. C. Moller, R. J. Berry, and T. D. Breitzman, J. Chem. Phys. **144**, 244904 (2016).

[26]R. A. Riggleman, H.-N. Lee, M. D. Ediger, and J. J. de Pablo, Phys. Rev. Lett. **99**, 215501 (2007).

[27]K. Yoshimoto, T. S. Jain, K. V. Workum, P. F. Nealey, and J. J. de Pablo, Phys. Rev. Lett. **93**, 175501 (2004).

[28]F. Léonforte, A. Tanguy, J. P. Wittmer, and J.-L. Barrat, Phys. Rev. Lett. **97**, 055501 (2006).

[29]D. Wang, Y. Liu, T. Nishi, and K. Nakajima, Appl. Phys. Lett. **100**, 251905 (2012).

[30]P. Friederich, F. Häse, J. Proppe, and A. Aspuru-Guzik, Nat. Mater. **20**, 750 (2021).

[31]J. C. Maier and N. E. Jackson, J. Chem. Phys. **157**, 174102 (2022).

[32]M. Wen, S. M. Blau, E. W. C. Spotte-Smith, S. Dwaraknath, and K. A. Persson, Chem. Sci. **12**, 1858 (2021).

[33]J. S. Smith, O. Isayev, and A. E. Roitberg, Chemical Science **8**, 3192 (2017).

[34]J. S. Smith, B. T. Nebgen, R. Zubatyuk, N. Lubbers, C. Devereux, K. Barros, S. Tretiak, O. Isayev, and A. E. Roitberg, Nat Commun **10**, 2903 (2019).

[35]H. J. Kulik, T. Hammerschmidt, J. Schmidt, S. Botti, M. A. L. Marques, M. Boley, M. Scheffler, M. Todorović, P. Rinke, C. Oses, A. Smolyanyuk, S. Curtarolo, A. Tkatchenko, A. P. Bartók, S. Manzhos, M. Ihara, T. Carrington, J. Behler, O. Isayev, M. Veit, A. Grisafi, J. Nigam, M. Ceriotti, K. T. Schütt, J. Westermayr, M. Gastegger, R. J. Maurer, B. Kalita, K. Burke, R. Nagai, R. Akashi, O. Sugino, J. Hermann, F. Noé, S. Pilati, C. Draxl, M. Kuban, S. Rigamonti, M. Scheidgen, M. Esters, D. Hicks, C. Toher, P. V. Balachandran, I. Tamblyn, S. Whitelam, C. Bellinger, and L. M. Ghiringhelli, Electron. Struct. **4**, 023004 (2022).

[36]V. L. Deringer, A. P. Bartók, N. Bernstein, D. M. Wilkins, M. Ceriotti, and G. Csányi, Chem. Rev. **121**, 10073 (2021).

[37]C.-I. Wang and N. E. Jackson, Chem. Mater. **35**, 1470 (2023).

[38]W. L. Jorgensen, D. S. Maxwell, and J. Tirado-Rives, J. Am. Chem. Soc. **118**, 11225 (1996).

[39]L. S. Dodda, I. Cabeza de Vaca, J. Tirado-Rives, and W. L. Jorgensen, Nucleic Acids Research **45**, W331 (2017).

[40]J. R. Gissinger, B. D. Jensen, and K. E. Wise, Polymer **128**, 211 (2017).

[41]A. P. Thompson, H. M. Aktulga, R. Berger, D. S. Bolintineanu, W. M. Brown, P. S. Crozier, P. J. in 't Veld, A. Kohlmeyer, S. G. Moore, T. D. Nguyen, R. Shan, M. J. Stevens, J. Tranchida, C. Trott, and S. J. Plimpton, Comp. Phys. Comm. **271**, 108171 (2022).

[42]G. S. Kedziora, S. A. Barr, R. Berry, J. C. Moller, and T. D. Breitzman, Theor Chem Acc **135**, 79 (2016).

[43]F. Neese, F. Wennmohs, U. Becker, and C. Riplinger, J. Chem. Phys. **152**, 224108 (2020).

[44]C. Ortiz, R. Kim, E. Rodighiero, C. K. Ober, and E. J. Kramer, Macromolecules **31**, 4074 (1998).

[45]M. Grandbois, M. Beyer, M. Rief, H. Clausen-Schaumann, and H. E. Gaub, Science **283**, 1727 (1999).

[46]S. Grimme, J. G. Brandenburg, C. Bannwarth, and A. Hansen, J. Chem. Phys. **143**, 054107 (2015).

[47]C. Bannwarth, S. Ehlert, and S. Grimme, J. Chem. Theory Comput. **15**, 1652 (2019).

[48]A. P. Bartók, R. Kondor, and G. Csányi, Phys. Rev. B **87**, 184115 (2013).

[49]S. De, A. P. Bartók, G. Csányi, and M. Ceriotti, Phys. Chem. Chem. Phys. **18**, 13754 (2016).

[50]J. Snoek, H. Larochelle, and R. P. Adams, "Practical Bayesian Optimization of Machine Learning Algorithms," (2012), arxiv:1206.2944 [cs, stat].

[51]C.-C. Chang and C.-J. Lin, ACM transactions on intelligent systems and technology (TIST) **2**, 1 (2011).

[52]C. Zhu, R. H. Byrd, P. Lu, and J. Nocedal, ACM Transactions on mathematical software (TOMS) **23**, 550 (1997).

[53]M. Kubát and S. Matwin, in *International Conference on Machine Learning* (1997).

[54]A. Giuntoli, N. K. Hansoge, A. van Beek, Z. Meng, W. Chen, and S. Keten, npj Comput Mater **7**, 1 (2021).

[55]Z. Meng, M. A. Bessa, W. Xia, W. Kam Liu, and S. Keten, Macromolecules **49**, 9474 (2016).